All - Inorganic CsPb1−xGexI2Br Perovskite with Enhanced Phase Stability and Photovoltaic Performance

COMMUNICATION

All-Inorganic $CsPb_{1-x}Ge_xI_2Br$ Perovskite with Enhanced Phase Stability and Photovoltaic Performance

Fu Yang*[a], Daisuke Hirotani[a], Gaurav Kapil[a], Muhammad Akmal Kamarudin[a], Chi Huey Ng[a], Yaohong Zhang[b], Qing Shen[b], Shuzi Hayase*[a]

Abstract: Compared with organic-inorganic perovskites, all-inorganic cesium based perovskites without volatile organic compounds have gained extensive interests because of the high thermal stability. However, they have a problem on phase transition from cubic phase (active for photo-electric conversion) to orthorhombic phase (inactive for photo-electric conversion) at room temperature, which has hindered further progress. Herein, novel inorganic $CsPb_{1-x}Ge_xI_2Br$ perovskites were prepared in humid ambient atmosphere without glovebox. The phase stability of the inorganic perovskite was effectively enhanced after germanium addition. In addition, highest power conversion efficiency of 10.8% with high open-circuit voltage (V_{OC}) of 1.27 V in planar solar cell based on $CsPb_{0.8}Ge_{0.2}I_2Br$ perovskite was achieved. Furthermore, highest V_{OC} up to 1.34 V was obtained by $CsPb_{0.7}Ge_{0.3}I_2Br$ perovskite which is a remarkable record in the field of inorganic perovskite solar cells. More importantly, all the photovoltaic parameters of $CsPb_{0.8}Ge_{0.2}I_2Br$ perovskite solar cells shows nearly no decay after 7 hours measurement in 50-60% relative humidity humid air without encapsulation.

Organometallic hybrid halide perovskite solar cells (PSCs) have attracted extensive attention over the past few years because of the ultra-electron mobility, long electron diffusion length and high optical absorption coefficient.[1] The power conversion efficiency have increased rapidly from initial 3.8% to 22.7% within just several years.[2] However, all the high performance perovskite solar cells typically include the organic group (i. e. methylammonium (MA^+), formamidinium (FA^+)), which restrict the perovskite solar cells development as the poor stability of the organic cation under the thermal, moisture and oxygen influence.[3] All-inorganic perovskites can solve those problems on the instability of perovskite solar cells with organic cations.[4] Until now, all-inorganic perovskite based on cesium cation ($CsMX_3$) is the most exploited material with high thermal stability and good photovoltaic performance.[5] $CsPbI_3$, $CsPbI_2Br$, $CsPbIBr_2$, $CsPbBr_3$ (have ranged bandgaps from ~1.73 to ~2.3 eV) are the most studied materials for the photovoltaic application. $CsPbBr_3$ which shows a good phase stability but has a wide bandgap (~2.3eV) which is not appropriate for the solar cell.[6] On the other hand, $CsPbI_3$ and $CsPbI_2Br$ have narrower bandgap (~1.73eV and ~1.92eV), but they shows phase transition from α phase (cubic, black phase and active for photo-electric conversion) to δ phase (orthorhombic, yellow phase, inactive for photo-electric conversion) at room temperature.[7] Thus, inorganic perovskite with good phase stability and proper bandgap is desirable. Furthermore, the fabrication process of PSCs is usually performed in a glovebox filled with nitrogen/argon to avoid moisture, oxidation and other uncontrolled influence which restrict the commercial application of perovskite solar cells.[8] Thus, it is requested hopefully to prepare high-quality inorganic perovskite films in the humid ambient air in order to lower the cost of fabrication. Inorganic perovskite, $CsPbI_2Br$ that has a narrower bandgap (~1.90 eV) than $CsPbBr_3$ and a better phase stability than $CsPbI_3$ is the most promising candidate material in the all-inorganic perovskite materials after balancing the bandgap and phase stability. However, the phase transition from cubic phase to orthorhombic phase occurs rapidly when kept in an uncontrolled air condition. Humidity has been proved to be the major issue for α phase stability of $CsPbI_2Br$.[9] Despite there are some reports on increasing the performance of $CsPbI_2Br$ based perovskite solar cells,[10] nearly none of them shows stability at high humidity condition. Furthermore, in most cases, the major component of the perovskite is still based on lead. Substitution of lead with less toxic material is significantly important as the use of lead is restricted in electronic devices according to the European regulations.[11] As far as we know there is no report regarding the preparation of $CsPbI_2Br$ based perovskite solar cells in ambient air condition at high humidity.

In this paper, for the first time, we reports photovoltaic performances for $CsPb_{1-x}Ge_xI_2Br$ (x, 0, 0.1, 0.2, 0.3) prepared at low temperature (160 °C) in humid air condition. The cubic phase stability was greatly increased by the incorporation of germanium. When the inorganic perovskite film without germanium was stored under 50~60% relative humidity, cubic phase of perovskite was changed to yellow orthorhombic phase rapidly within 10 minutes. However, the cubic phase of the perovskite was still kept nearly no change after 120 h measurement for the $CsPb_{0.8}Ge_{0.2}I_2Br$ perovskite film. With the increasing germanium in the inorganic perovskite, the V_{OC} was greatly increased from 1.02 V of $CsPbI_2Br$, to 1.34 V of $CsPb_{0.7}Ge_{0.3}I_2Br$, which might be a record V_{OC} for $CsPbI_2Br$-based solar cells. In addition, the champion efficiency of 10.8% was obtained by the planar perovskite solar cell with a structure of $FTO/SnO_2/CsPb_{0.8}Ge_{0.2}I_2Br$/P3HT/Spiro/Au along with a high V_{OC} of 1.27 V. The stability of the solar cells was greatly increased with the parameters including short circuit current, V_{OC}, fill factor and efficiency of $CsPb_{0.8}Ge_{0.2}I_2Br$ perovskite solar cells showed nearly no decay after measured for more than 7 hours in 50-60% RH humid air without encapsulation.

Figure 1a shows XRD patterns of $CsPb_{1-x}Ge_xI_2Br$ with different Ge content (x, 0, 0.1, 0.2, 0.3). All the films were prepared on the glass substrates by one-step anti-solvent spin-coating method in

[a] F. Yang, D. Hirotani, Dr. G. Kapil, Dr. M. A. Kamarudin, Dr. C. H. Ng Prof. Dr. S. Hayase
Graduate School of Life Science and Systems Engineering
Institution Kyushu Institute of Technology
2-4 Hibikino Wakamatsu-ku, Kitakyushu 808-0196, Japan
E-mail: yang-fu@edu.life.kyutech.ac.jp; hayase@life.kyutech.ac.jp
[b] Dr. Y. H. Zhang, Prof. Dr. Q. Shen
Department Graduate School of Informatics and Engineering
University of Electro-Communications
1-5-1 Chofugaoka, Chofu, Tokyo 182-8585, Japan
Supporting information for this article is given via a link at the end of the document.

ambient air condition with high humidity.[12] The film preparation process is illustrated in Figure S1. Strong diffraction peaks located at 14.6°, 20.8° and 29.5° were observed corresponding to the (100), (110) and (200) planes of cubic phase of $CsPbI_2Br$, which are in good agreement with previous reports.[13] These results indicate that all the $CsPb_{1-x}Ge_xI_2Br$ perovskite films are all highly crystallized perovskite phase. Meanwhile, a typical orthorhombic phase at 10.0° was found in the $CsPbI_2Br$ perovskite film.[9] In contrast, no peak assigned to the orthorhombic phase was observed upon incorporation of germanium into the perovskite, which is clearly shown in the zoomed image in Figure S3a. These results showed that the germanium addition directly increase the cubic phase stability of $CsPbI_2Br$. With addition of Ge, crystallite size calculated from XRD is decreased from 69.7 nm for x=0 to 35.3 nm for x= 0.1, 32.6 nm for x= 0.2, and 23.8 nm for x= 0.3. Top view scanning electron microscopy (SEM) images of the $CsPb_{1-x}Ge_xI_2Br$ films shown in Figure S7 exhibit obvious decreased crystal grain size which is in agreement with the XRD data. The reduced crystal size could induce lattice strain to stabilize the α phase of $CsPbI_2Br$.[5a, 10a] Atomic force microscopy (AFM) images in Figure S13 clearly show the smoother perovskite film for the $CsPb_{0.8}Ge_{0.2}I_2Br$ (Rq=3.0) compared to the pristine $CsPbI_2Br$ (Rq=15.2), which could enhance the performance of perovskite devices by providing better interfacial contact with the hole transport layer.

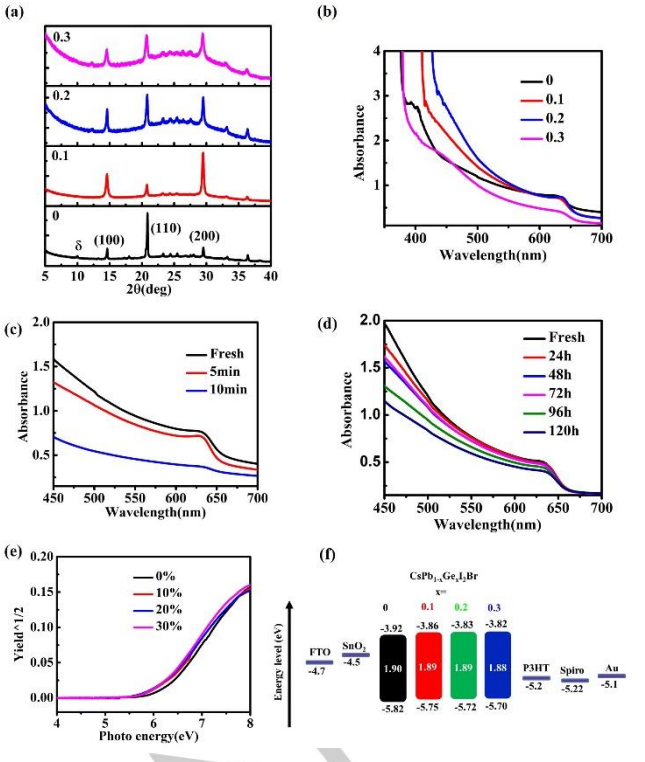

Figure 1. (a) XRD spectra of fresh $CsPb_{1-x}Ge_xI_2Br$ perovskite films on glass substrates(x, 0, 0.1, 0.2, 0.3) and the corresponding (b) UV-vis spectra. (c) UV-vis spectra of $CsPbI_2Br$ perovskite film measured in ambient air at 50~60% RH over a period of time. (d) UV-vis spectra of $CsPb_{0.8}Ge_{0.2}I_2Br$ perovskite film measured in ambient air at 50~60% RH over a period of time. (e) Photoelectron yield spectroscopy (PYS) measurement for $CsPb_{1-x}Ge_xI_2Br$ perovskite film (x, 0, 0.1, 0.2, 0.3) measured on FTO substrates. (f) Energy band diagram constructed from Uv-vis and PYS measurement.

The optical properties of the $CsPb_{1-x}Ge_xI_2Br$ perovskite materials were evaluated by the UV-vis measurement, shown in Figure 1b. The absorption edges shifted to a slight longer wavelength as the germanium content increases which clearly shown in Figure S3b. The absorption intensity was increased as Ge content increased from 0, 0.1, to 0.2 and decreased at the Ge content of 0.3. The film stability of the perovskite film in 50-60% RH humid air atmosphere was measured and the results are shown in Figure 1c and 1d. For the $CsPbI_2Br$, the cubic phase absorption edge at around 630 nm decreased rapidly within 10 minutes. However, for the $CsPb_{0.8}Ge_{0.2}I_2Br$ perovskite, the cubic phase absorption edge showed no change even after 120 hours. The XRD pattern change of the $CsPb_{1-x}Ge_xI_2Br$ perovskite materials kept in ambient air for different time is shown Figure S4. Similar to the results obtained from UV-Vis measurement, the cubic phase stability is enhanced upon addition of germanium as evidenced from the XRD spectra. The band gaps, Eg for the perovskite materials are calculated form the Tauc plot shown in Figure S5, where the E_g was 1.901, 1.894, 1.889, and 1.881 eV for x = 0, 0.1, 0.2 and 0.3, respectively. Valence band of the perovskite materials was determined from photoelectron yield spectroscopy (PYS), shown in Figure 1e. Valence band edge slightly shifted from -5.82 of x= 0 to negative values of -5.75, -5.72 and -5.70 eV for x= 0.1, 0.2 and 0.3, respectively. The energy band diagram was constructed using Eg and valence band values shown in Figure 1f. Upon increasing the Ge content, both the balance band and conduction band of $CsPbI_2Br$ were upshifted which is similar to our previous reports. [12]

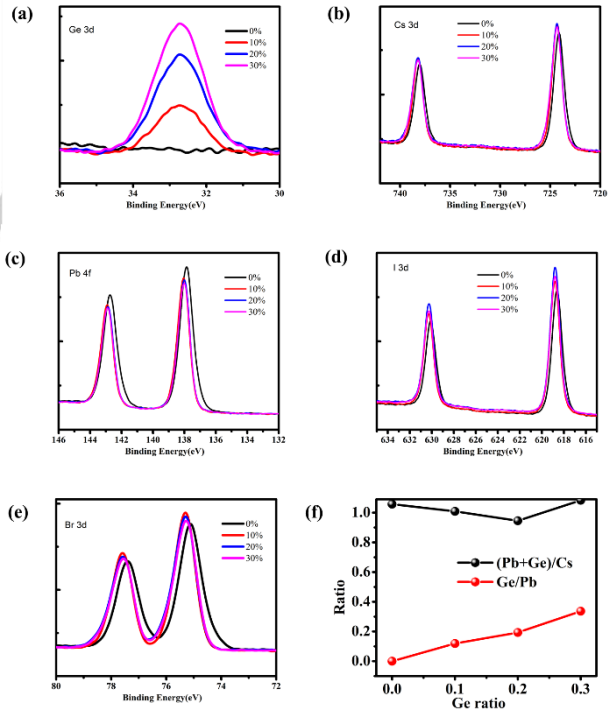

Figure 2. XPS core level spectra for $CsPb_{1-x}Ge_xI_2Br$ (X, 0, 0.1, 0.2, 0.3). (a) Ge 3d, (b) Cs 3d, (c) Pb 4f, (d) I 3d, (e) Br 3d. (f) The ratio of GeI_2 added initially (Horizontal line) vs. Molar ratio of Ge/Pb and (Pb+Ge)/ Cs in the film from the XPS spectra (Vertical line).

Figure S6 shows the wide scan spectra of X-ray photoelectron spectra (XPS) for the perovskite films. The binding energy peak

at 32.7 eV corresponding to the Ge 3d core levels significantly increased with the increasing content of Ge content, indicating that the Ge has been successfully incorporated into the perovskite film (Figure 2a). Figure 2b, 2c, 2d and 2e, show the Cs 3d, Pb 4f, I 3d and Br 3d core levels. Notably, in the Ge-incorporated $CsPbI_2Br$ films, the peaks of Cs 3d and Pb 4f are slightly shifted to higher binding energy, which is consistent with the previous reports on metal-substituted $CsPbI_2Br$ perovskite.[10d, 10e] It has been reported that the binding energy of Pb cation and halides are not changed by a little fluctuating on ratio of I/Br in mixed-halide perovskites, nor simple physical mixing.[14] Therefore, the origin of the shifts comes from the changes in the chemical bonding between Cs and Pb cation, which are associated with the influence of Ge. In addition, the Br 3d peaks of $CsPbI_2Br$ decreased slightly when Ge is added. The Ge/Pb and (Pb+Ge)/Cs ratios are calculated from the XPS spectra as shown in Figure 2f. The ratio of (Pb+Ge)/Cs is calculated to be close to 1.0, suggesting that Ge is substituting the Pb atoms. Figure S9a and 9b show the steady state photoluminescence (PL) and time-resolved PL (TRPL) of the $CsPb_{1-x}Ge_xI_2Br$ perovskite film on glass substrates. As shown in Figure 8a, the PL peaks centers of $CsPb_{1-x}Ge_xI_2Br$ perovskite showed a redshift with the increasing Ge content. The TRPL curves were fitted by the double exponential decay function. The presence of fast decay component τ_1 was attributed to indicate the bimolecular recombination, and the slow decay component τ_2 was assigned to effective recombination lifetime. The detail parameters of PL lifetime are summarized in table S1. The calculated τ_2 of the $CsPbI_2Br$, $CsPb_{0.9}Ge_{0.1}I_2Br$, $CsPb_{0.8}Ge_{0.2}I_2Br$, and $CsPb_{0.7}Ge_{0.3}I_2Br$ films was 2.40, 3.02, 20.62 and 8.56 ns, respectively. The increased τ_2 suggesting a better effective recombination lifetime, when incorporating Ge in the $CsPbI_2Br$ perovskite, especially for the $CsPb_{0.8}Ge_{0.2}I_2Br$ perovskite.

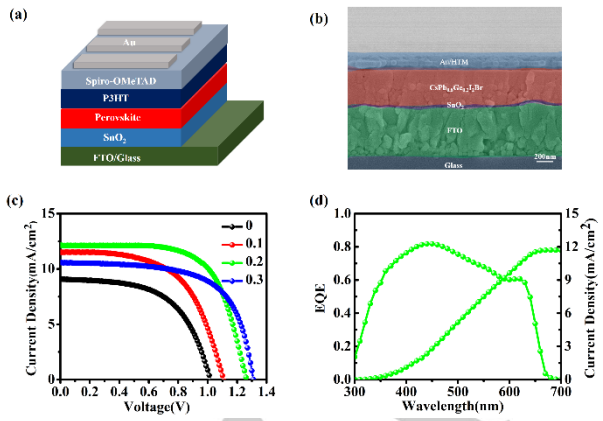

Figure 3. (a) Schematic structure and (b) cross sectional SEM image of planar perovskite device. (c) J-V curve in reverse scan for champion $CsPb_{1-x}Ge_xI_2Br$ perovskite solar cell. (d) IPCE spectra and the corresponding integrated current density of $CsPb_{0.8}Ge_{0.2}I_2Br$ PSC.

Table 1. Photovoltaic parameters of champion planar PSCs devices.

Materials	V_{OC}(V)	J_{sc}(mA/cm^2)	FF(%)	PCE(%)
$CsPbI_2Br$	1.02	9.06	57.2	5.3
$CsPb_{0.9}Ge_{0.1}I_2Br$	1.11	11.39	59.3	7.6
$CsPb_{0.8}Ge_{0.2}I_2Br$	1.27	12.15	70.1	10.8
$CsPb_{0.7}Ge_{0.3}I_2Br$	1.32	10.58	64.5	9.0

The effect of Ge substitution on the PSCs performance is investigated with the planar PSC structure of FTO/SnO_2/Perovskite/P3HT/Spiro/Au. All the process of PSCs are performed in ambient air condition at high humidity. Figure 3a and 3b show the schematic structure and cross-sectional SEM image of the device. The photovoltaic parameters are listed in Table 1 and the current density-voltage (J-V) curves of the PSCs are shown Figure 3c. The solar cell based on $CsPbI_2Br$ showed the lowest power conversion efficiency (PCE) with 5.3% with a low open-circuit potential (V_{OC}) of 1.02 V. Upon Ge incorporation, the V_{OC} was increased gradually to 1.11V for $CsPb_{0.9}Ge_{0.1}I_2Br$, 1.27 V for $CsPb_{0.8}Ge_{0.2}I_2Br$ and 1.32 V for $CsPb_{0.7}Ge_{0.3}I_2Br$. The champion V_{OC} for $CsPb_{0.7}Ge_{0.3}I_2Br$ was up to 1.34 V which is the highest ever reported for the $CsPbI_2Br$ based perovskite devices. Moreover, the J_{SC} was increased from 9.06 mA/cm^2 to 11.39 mA/cm^2 for $CsPb_{0.9}Ge_{0.1}I_2Br$ and 12.15 mA/cm^2 for $CsPb_{0.8}Ge_{0.2}I_2Br$. However, the J_{SC} decreased to 10.58 mA/cm^2 for $CsPb_{0.7}Ge_{0.3}I_2Br$, which is consistent with the absorbance spectra. In addition, the fill factor (FF) also showed a greatly improved when Ge was incorporated as evidenced from Table 1. The highest efficiency was achieved by $CsPb_{0.8}Ge_{0.2}I_2Br$ with the PCE of 10.8%, which could be a world record for this type of perovskite prepared in ambient atmosphere at high humidity. In addition, Ge incorporated perovskite with a broad band gap of ~1.9 V and a comparable V_{OC} around 1.3 V could be a good candidate applying in perovskite/silicon and perovskite/perovskite tandem solar cells.[15] Next, The electrochemical impedance spectroscopy measurements were performed to study the charge-transfer mechanism at the interfaces of the PSC devices. The Nyquist plots of $CsPbI_2Br$, $CsPb_{0.8}Ge_{0.2}I_2Br$ perovskite based solar cell devices are shown in Figure S10. As it is known that lower Rs suggests a better electro transport and larger R_{rec} implies the lower recombination rate. According to Figure S10, the solar cell device based on $CsPb_{0.8}Ge_{0.2}I_2Br$ has a much higher R_{rec} than that of $CsPbI_2Br$ which determined from the width of the semicircle, suggesting the recombination rate is decreased by Ge incorporation.[16] Therefore, it can be concluded that the larger Rrec of Ge incorporated perovskite device indicates that the carrier mobility in correspondent device is improved thus leading to enhanced V_{oc} and FF.

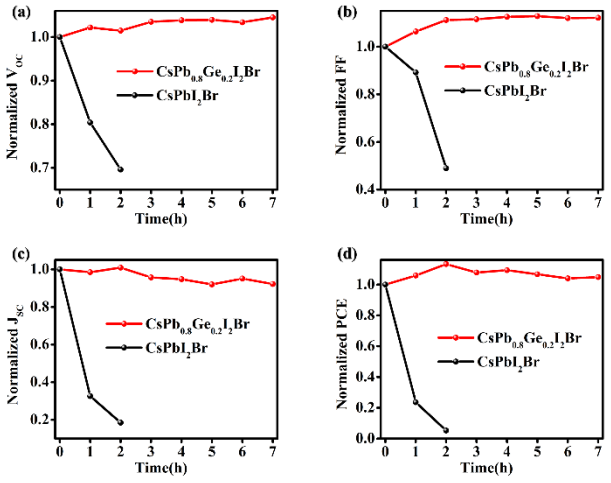

Figure 4. Stability test of $CsPbI_2Br$ and $CsPb_{0.8}Ge_{0.2}I_2Br$ PSCs without sealing in 50-60% RH ambient atmosphere. (a) Voc. (b) FF. (c) J_{SC}. (d) PCE.

Stability of $CsPbI_2Br$ and $CsPb_{0.8}Ge_{0.2}I_2Br$ PSCs is investigated and the result is shown in Figure 4. As shown in Figure 4d, the PCE of $CsPbI_2Br$ deceased rapidly to nearly 0 within 2 hours along with the rapid decreasing of V_{OC}, J_{SC} and FF. However, the PCE of $CsPb_{0.8}Ge_{0.2}I_2Br$ kept no decline over 7 hours. In addition, all the parameters including V_{OC}, J_{SC} and FF kept nearly no dropping over 7 hours measurement. The above results shows that incorporation of Ge into the $CsPbI_2Br$ perovskite enhanced the photovoltaic performances and gave stability against the phase transition for all-inorganic perovskite.

In conclusion, novel all-inorganic $CsPb_{1-x}Ge_xI_2Br$ (x, 0, 0.1, 0.2, 0.3) perovskites is successfully prepared in ambient temperature at high humidity. The cubic phase stability of the all-inorganic perovskite with germanium was effectively enhanced. The all-inorganic perovskite with Ge shows a better effective recombination lifetime and low trap densities. Moreover, incorporation of Ge increased the V_{OC}, leading to the highest V_{OC} of up to 1.34 V for $CsPb_{0.7}Ge_{0.3}I_2Br$ perovskite solar cells. The highest power conversion efficiency of 10.8 % with high open-circuit voltage (V_{OC}) of 1.27 V in planar solar cell based on $CsPb_{0.8}Ge_{0.2}I_2Br$ perovskite was achieved. At last, all the parameters including short circuit current, V_{OC}, fill factor and efficiency of $CsPb_{0.8}Ge_{0.2}I_2Br$ perovskite solar cells was kept after the samples were measured for more than 7 hour in 50-60% relative humidity humid air without encapsulation. This research gives a good direction for preparing stable all-inorganic perovskite devices in ambient condition and has the prospect to be used in tandem solar cells due to the high V_{OC}.

Acknowledgements

The authors acknowledge JST Mirai Program for financial support.

Conflict of interest

The authors declare no conflict of interest.

Keywords: inorganic perovskite • germanium iodide • phase stability • solar cell • lead substitute

[1] a) M. M. Lee, J. Teuscher, T. Miyasaka, T. N. Murakami, H. J. Snaith, Science 2012, 338, 643-647; b) T. Leijtens, G. E. Eperon, S. Pathak, A. Abate, M. M. Lee, H. J. Snaith, Nature communications 2013, 4, 2885; c) W. Shockley, H. J. Queisser, Journal of applied physics 1961, 32, 510-519.

[2] a) A. Kojima, K. Teshima, Y. Shirai, T. Miyasaka, Journal of the American Chemical Society 2009, 131, 6050-6051; b) W. S. Yang, B.-W. Park, E. H. Jung, N. J. Jeon, Y. C. Kim, D. U. Lee, S. S. Shin, J. Seo, E. K. Kim, J. H. Noh, Science 2017, 356, 1376-1379.

[3] a) J. S. Manser, M. I. Saidaminov, J. A. Christians, O. M. Bakr, P. V. Kamat, Accounts of chemical research 2016, 49, 330-338; b) S. Wang, Y. Jiang, E. J. Juarez-Perez, L. K. Ono, Y. Qi, Nature Energy 2017, 2, 16195; c) H. Tsai, W. Nie, J.-C. Blancon, C. C. Stoumpos, R. Asadpour, B. Harutyunyan, A. J. Neukirch, R. Verduzco, J. J. Crochet, S. Tretiak, Nature 2016, 536, 312.

[4] a) D. Jialong, H. Tianyu, Z. Yuanyuan, H. Benlin, T. Qunwei, Angewandte Chemie International Edition 2018, 57, 5746-5749; b) J. Liang, P. Zhao, C. Wang, Y. Wang, Y. Hu, G. Zhu, L. Ma, J. Liu, Z. Jin, Journal of the American Chemical Society 2017, 139, 14009-14012; c) N. Li, Z. Zhu, J. Li, A. K. Y. Jen, L. Wang, Advanced Energy Materials 2018, 1800525.

[5] a) G. E. Eperon, G. M. Paterno, R. J. Sutton, A. Zampetti, A. A. Haghighirad, F. Cacialli, H. J. Snaith, Journal of Materials Chemistry A 2015, 3, 19688-19695; b) L. Protesescu, S. Yakunin, M. I. Bodnarchuk, F. Krieg, R. Caputo, C. H. Hendon, R. X. Yang, A. Walsh, M. V. Kovalenko, Nano letters 2015, 15, 3692-3696.

[6] J. Duan, Y. Zhao, B. He, Q. Tang, Angewandte Chemie 2018, 130, 3849-3853.

[7] a) C. Liu, W. Li, C. Zhang, Y. Ma, J. Fan, Y. Mai, Journal of the American Chemical Society 2018, 140, 3825-3828; b) N. J. Jeon, J. H. Noh, Y. C. Kim, W. S. Yang, S. Ryu, S. I. Seok, Nature materials 2014, 13, 897; c) A. Swarnkar, A. R. Marshall, E. M. Sanehira, B. D. Chernomordik, D. T. Moore, J. A. Christians, T. Chakrabarti, J. M. Luther, Science 2016, 354, 92-95; d) S. Sharma, N. Weiden, A. Weiss, Zeitschrift für Physikalische Chemie 1992, 175, 63-80.

[8] a) B. J. Kim, D. H. Kim, Y.-Y. Lee, H.-W. Shin, G. S. Han, J. S. Hong, K. Mahmood, T. K. Ahn, Y.-C. Joo, K. S. Hong, Energy & Environmental Science 2015, 8, 916-921; b) S. N. Habisreutinger, T. Leijtens, G. E. Eperon, S. D. Stranks, R. J. Nicholas, H. J. Snaith, Nano letters 2014, 14, 5561-5568.

[9] S. Mariotti, O. S. Hutter, L. J. Phillips, P. J. Yates, B. Kundu, K. Durose, ACS Applied Materials & Interfaces 2018, 10, 3750-3760.

[10] a) Z. Zeng, J. Zhang, X. Gan, H. Sun, M. Shang, D. Hou, C. Lu, R. Chen, Y. Zhu, L. Han, Advanced Energy Materials 2018, 1801050; b) L. Yan, Q. Xue, M. Liu, Z. Zhu, J. Tian, Z. Li, Z. Chen, Z. Chen, H. Yan, H. L. Yip, Advanced Materials 2018, 1802509; c) D. Bai, J. Zhang, Z. Jin, H. Bian, K. Wang, H. Wang, L. Liang, Q. Wang, S. F. Liu, ACS Energy Letters 2018, 3, 970-978; d) J. K. Nam, S. U. Chai, W. Cha, Y. J. Choi, W. Kim, M. S. Jung, J. Kwon, D. Kim, J. H. Park, Nano letters 2017, 17, 2028-2033; e) C. F. J. Lau, M. Zhang, X. Deng, J. Zheng, J. Bing, Q. Ma, J. Kim, L. Hu, M. A. Green, S. Huang, A. Ho-Baillie, ACS Energy Letters 2017, 2, 2319-2325.

[11] J. Rödel, W. Jo, K. T. Seifert, E. M. Anton, T. Granzow, D. Damjanovic, Journal of the American Ceramic Society 2009, 92, 1153-1177.

[12] F. Yang, G. Kapil, P. Zhang, Z. Hu, M. A. Kamarudin, T. Ma, S. Hayase, ACS applied materials & interfaces 2018.

[13] a) R. J. Sutton, G. E. Eperon, L. Miranda, E. S. Parrott, B. A. Kamino, J. B. Patel, M. T. Hörantner, M. B. Johnston, A. A. Haghighirad, D. T. Moore, Advanced Energy Materials 2016, 6; b) C. Y. Chen, H. Y. Lin, K. M. Chiang, W. L. Tsai, Y. C. Huang, C. S. Tsao, H. W. Lin, Advanced materials 2017, 29, 1605290; c) W. Li, M. U. Rothmann, A. Liu, Z. Wang, Y. Zhang, A. R. Pascoe, J. Lu, L. Jiang, Y. Chen, F. Huang, Advanced Energy Materials 2017, 7.

[14] a) M. Saliba, T. Matsui, J.-Y. Seo, K. Domanski, J.-P. Correa-Baena, M. K. Nazeeruddin, S. M. Zakeeruddin, W. Tress, A. Abate, A. Hagfeldt, Energy & Environmental Science 2016, 9, 1989-1997; b) W. Xu, L. Zheng, X. Zhang, Y. Cao, T. Meng, D. Wu, L. Liu, W. Hu, X. Gong, Advanced Energy Materials 2018, 8, 1703178.

[15] a) H. Shen, T. Duong, Y. Wu, J. Peng, D. Jacobs, N. Wu, K. Weber, T. White, K. Catchpole, Science and Technology of Advanced Materials 2018, 19, 53-75; b) R. Fan, N. Zhou, L. Zhang, R. Yang, Y. Meng, L. Li, T. Guo, Y. Chen, Z. Xu, G. Zheng, Solar RRL 2017, 1, 1700149; c) T. Leijtens, K. A. Bush, R. Prasanna, M. D. McGehee, Nature Energy 2018; d) N. N. Lal, Y. Dkhissi, W. Li, Q. Hou, Y. B. Cheng, U. Bach, Advanced Energy Materials 2017, 7, 1602761; e) G. E. Eperon, T. Leijtens, K. A. Bush, R. Prasanna, T. Green, J. T.-W. Wang, D. P. McMeekin, G. Volonakis, R. L. Milot, R. May, Science 2016, 354, 861-865.

[16] Y. Fu, K. M. Akmal, Z. Putao, K. Gaurav, M. Tingli, H. Shuzi, ChemSusChem 2018, 11, 2348-2357.

COMMUNICATION

Germanium is first reported to incorporate in all-inorganic $CsPbI_2Br$ perovskite leading to the enhanced phase stability and photovoltaic performance. Large V_{OC} of up to 1.34 V and high PCE of 10.8% were achieved by planar perovskite solar cells (PSCs) that prepared in uncontrolled humid air atmosphere without glovebox, which are remarkable records for the $CsPbI_2Br$ PSCs.

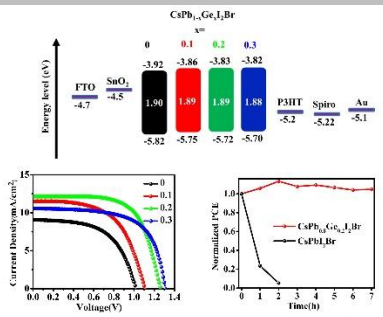

*F. Yang, D. Hirotani, G. Kapil, M. A. Kamarudin, C. H. Ng, Y. H. Zhang, Q. Shen, S. Hayase**

Page 1 – Page 4

All-Inorganic $CsPb_{1-x}Ge_xI_2Br$ Perovskite with Enhanced Phase Stability and Photovoltaic

COMMUNICATION

All-Inorganic $CsPb_{1-x}Ge_xI_2Br$ Perovskite with Enhanced Phase Stability and Photovoltaic Performance

Fu Yang*[a], Daisuke Hirotani[a], Gaurav Kapil[a], Muhammad Akmal Kamarudin[a], Chi Huey Ng[a], Yaohong Zhang[b], Qing Shen[b], Shuzi Hayase*[a]

[a] F. Yang, D. Hirotani, Dr. G. Kapil, Dr. M. A. Kamarudin, Dr. C. H. Ng Prof. Dr. S. Hayase
Graduate School of Life Science and Systems Engineering Institution Kyushu Institute of Technology 2-4 Hibikino Wakamatsu-ku, Kitakyushu 808-0196, Japan
E-mail: yang-fu@edu.life.kyutech.ac.jp; hayase@life.kyutech.ac.jp
[b] Dr. Y. H. Zhang, Prof. Dr. Q. Shen
Department Graduate School of Informatics and Engineering
University of Electro-Communications 1-5-1 Chofugaoka, Chofu, Tokyo 182-8585, Japan

Experimental Section

Preparation of perovskite solar cells

All reagents including ethyl acetate (Aldrich, 99.8 %) and chlorobenzene (Aldrich, 99.8%) were used without further purification. F-doped SnO_2 (FTO glass, Nippon Sheet Glass Co. Ltd) substrates were first patterned and cleaned using zinc powder and 6 N hydrochloric acid solution. Tin (II) chloride (Aldrich, 98 %) was dissolved in ethanol (Wako, 99.8 %) to form 0.1 M $SnCl_2$ solution. Then the $SnCl_2$ solution was spin-coated on the cleaned FTO glass in turn at 2000 rpm for 30 seconds and 6000rpm 30s. The substrate was annealed at 180 °C for 60 minutes on a hot plate to form a dense SnO_2 electron transport layer. Proper molar ratio of CsBr (TCI, 98 %) and PbI_2 (TCI, 99.99 %) and GeI_2 (Aldrich, 99%) were dissolved in anhydrous dimethylformamide (DMF, Aldrich, 99.8 %) and anhydrous dimethyl sulfoxide (DMSO, Aldrich, 99.8 %) (DMF: DMSO, 3:7) to prepare 1.4 M $CsPb_{1-x}Ge_xI_2Br$ precursor solution. The perovskite precursor solution was spin-coated on SnO_2-coated substrate at 3000 rpm for 25 seconds and ethyl acetate (0.5 ml) was dripped on the substrate 15 seconds after starting the spin-coating process, followed by heating at 160 °C for 10 minutes. Then 5mg/mL P3HT(TCI, 99%) chlorobenzene solution was spin-coating at 4000rpm for 25 seconds and annealed at 160 °C for 10 minutes. The Spiro-MeOTAD layer was then prepared by spin-coating a chlorobenzene solution containing 180 mM Spiro-MeOTAD (Aldrich, 99 %), 60 mM tert-butylpyridine

(Aldrich, 96 %), 30 mM Li-TFSI (Aldrich, 99.95 %) (520 mg/mL in acetonitrile) and 33 mM FK209 (Aldrich, 99 %) (300 mg/mL in acetonitrile) at 4000 rpm for 30 seconds. Finally, 80 nm-thick Au counter electrode was deposited by thermal evaporation. All procedures were performed at around 50%-60% relative humidity in ambient air condition (Relative humidity was recorded using a hygrometer accurate to ± 5 % RH between 25 % and 69.9 % RH, ±10 % RH between 70 % and 90 % RH) (A&D Company, AD-5681)).

Characterization

Solar cell performance was measured by a solar simulator (CEP-2000SRR, Bunkoukeiki Inc., AM 1.5G 100 $mWcm^{-2}$) and a mask with exposure area 0.10 cm^2 was used during the photovoltaic measurements with a 0.1 V/s scanning rate in reverse (from the open-circuit voltage (V_{OC}) to the short-current density (J_{SC})) and forward (from J_{SC} to V_{OC}) modes under standard global AM 1.5 illumination. The IPCE spectra were recorded using a monochromatic Xenon lamp (Bunkouki CEP-2000SRR). X-ray Diffraction (XRD) Study. The surface morphology of the samples was observed through a scanning electron microscope (SEM) (JEOL, Neoscope, JCM-6000). The XRD patterns were obtained by a Rigaku Smartlab X-ray diffractometer with monochromatic Cu-Kβ irradiation (45 kV/200 mA). The UV-Vis measurement was performed using a JASCO V-670. Spectrophotometer. Electrochemical impedance spectroscopic (EIS) measurements were performed in the dark using an electrochemical workstation with a frequency range from 1 Hz to 1 MHz at 0.7 V applied bias. Photoelectron yield spectroscopy (PYS) was used to determine the valence band using a Bunkoukeiki KV205-HK ionization energy measurement system with – 5.0 V of applied voltage under 10^{-4} Pa vacuum.

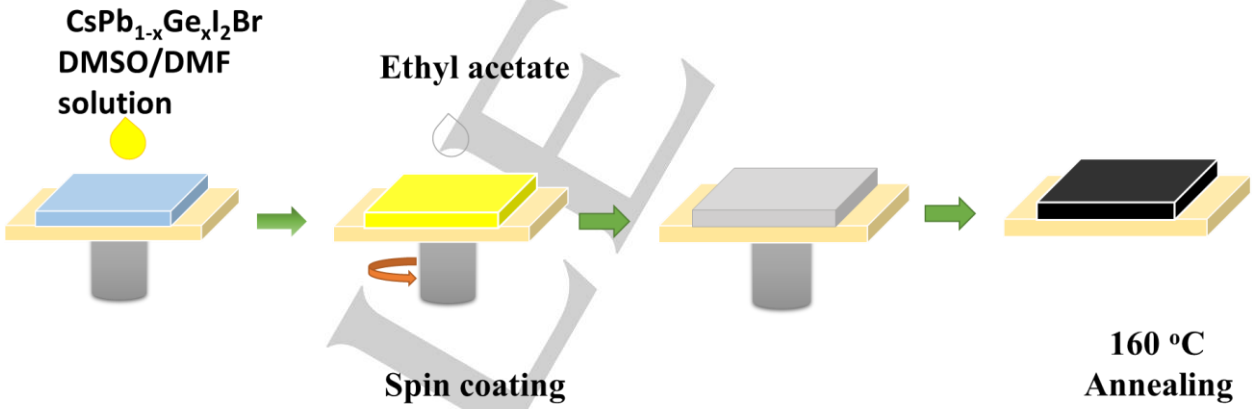

Figure S1 Schematic illustration of the one-step process using anti-solvent for fabricating perovskite films.

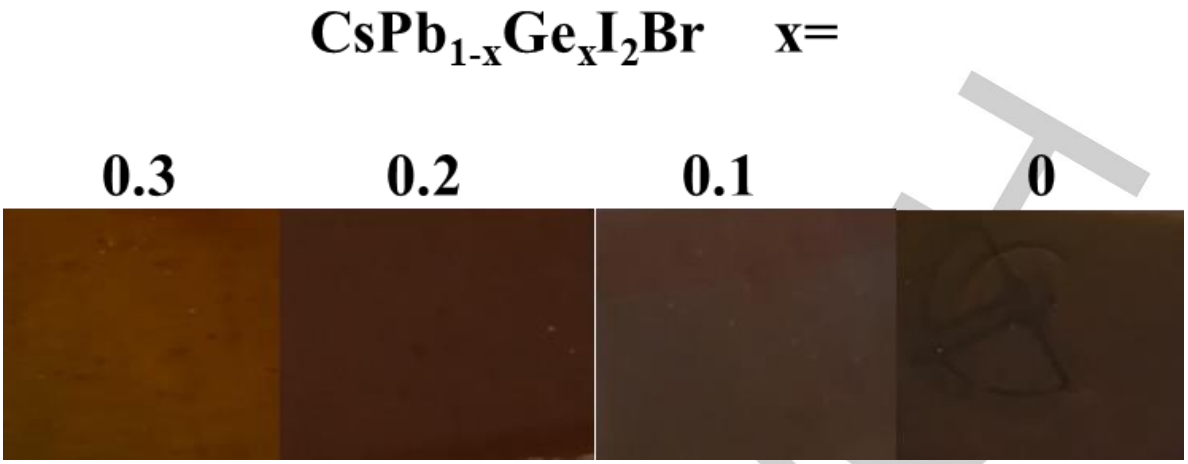

Figure S2 Optical images of $CsPb_{1-x}Ge_xI_2Br$ perovskite films.

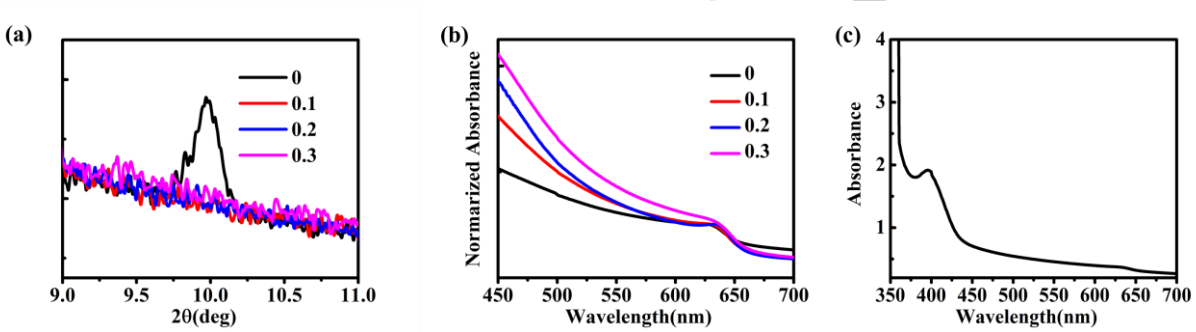

Figure S3 (a) Narrow scale for the δ phase from the XRD of the $CsPb_{1-x}Ge_xI_2Br$ perovskite film (x, 0, 0.1, 0.2, 0.3). (b) Namarized absoebance of $CsPb_{1-x}Ge_xI_2Br$ perovskite film. (c) UV-vis absorbance of $CsPbI_2Br$ perovskite film after kept in 50-60% RH humid air atmosphere for 10 minutes.

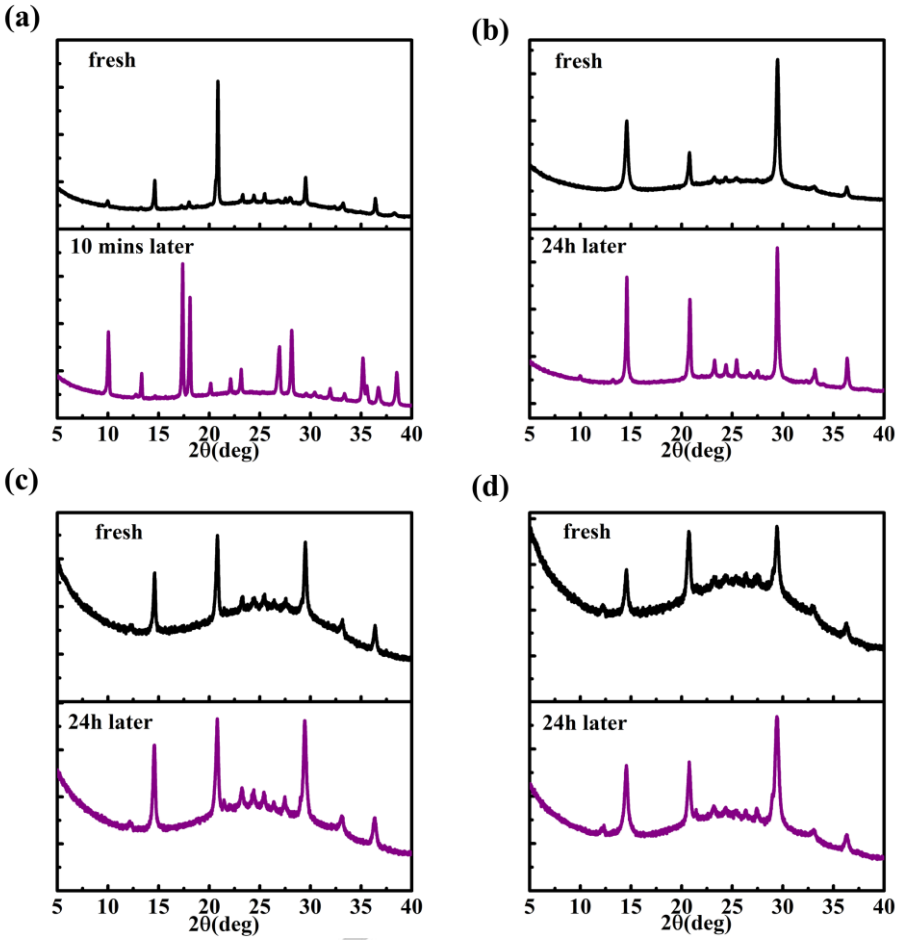

Figure S4 XRD spectra of the $CsPb_{1-x}Ge_xI_2Br$ perovskite film (x, 0, 0.1, 0.2, 0.3) measure at different time. (a) $CsPbI_2Br$ perovskite, (b) $CsPb_{0.9}Ge_{0.1}I_2Br$ perovskite, (c) $CsPb_{0.8}Ge_{0.2}I_2Br$ perovskite, (b) $CsPb_{0.7}Ge_{0.3}I_2Br$ perovskite.

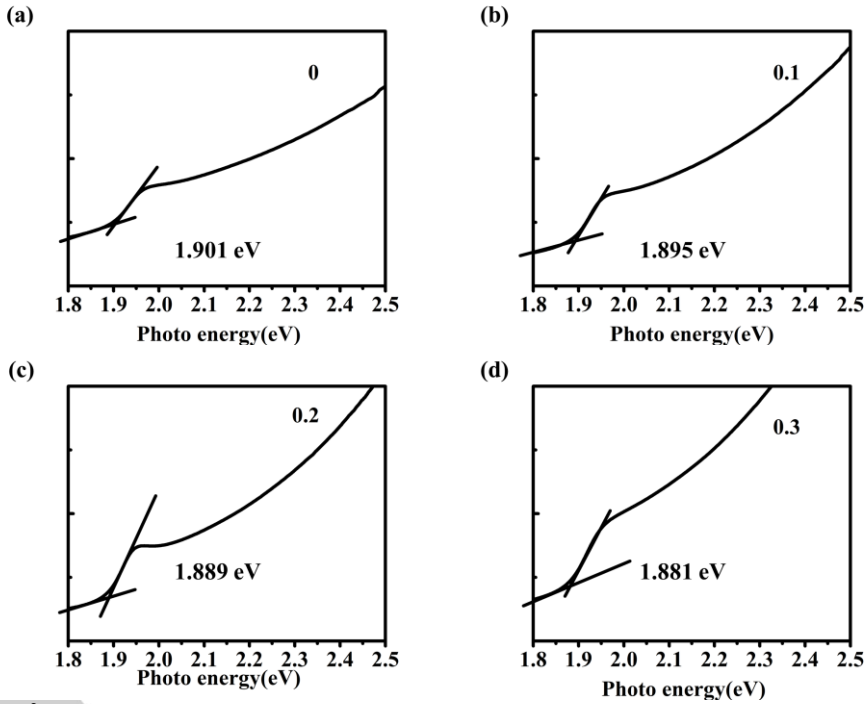

Figure S5 $(\alpha h\nu)^2$ versus light excitation energy $h\nu$. (a) $CsPbI_2Br$ perovskite, (b) $CsPb_{0.9}Ge_{0.1}I_2Br$ perovskite, (c) $CsPb_{0.8}Ge_{0.2}I_2Br$ perovskite, (b) $CsPb_{0.7}Ge_{0.3}I_2Br$ perovskite.

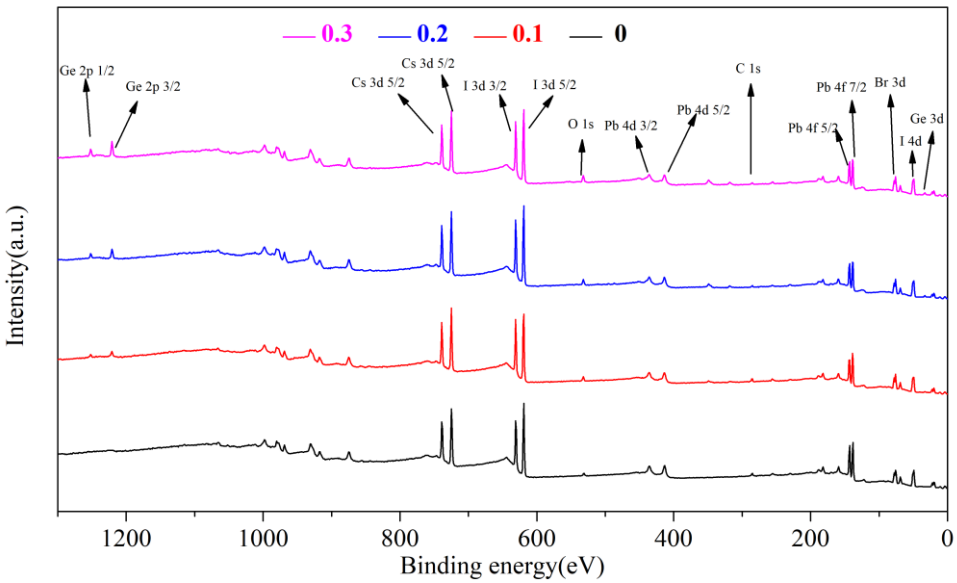

Figure S6 Wide scan XPS spectra $CsPb_{1-x}Ge_xI_2Br$ perovskite film (x, 0, 0.1, 0.2, 0.3).

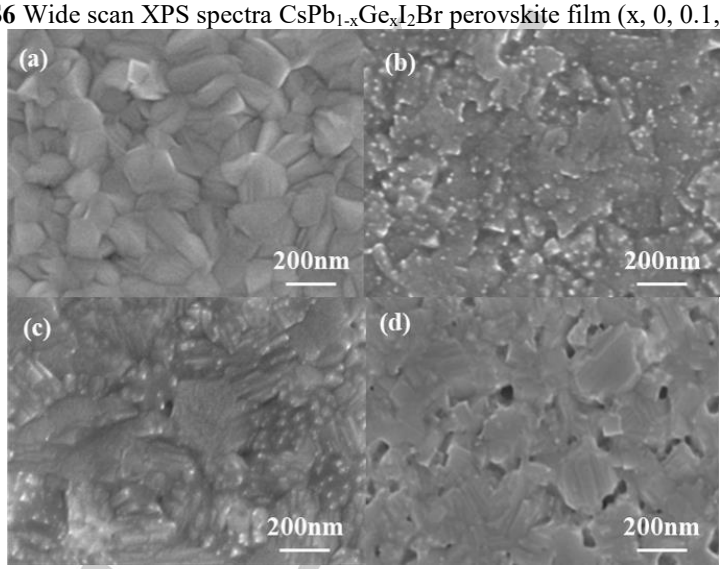

Figure S7 SEM images of $CsPb_{1-x}Ge_xI_2Br$ perovskite film (x, 0, 0.1, 0.2, 0.3) on FTO/SnO_2 substrates. a) $CsPbI_2Br$ perovskite, (b) $CsPb_{0.9}Ge_{0.1}I_2Br$ perovskite, (c) $CsPb_{0.8}Ge_{0.2}I_2Br$ perovskite, (d) $CsPb_{0.7}Ge_{0.3}I_2Br$ perovskite.

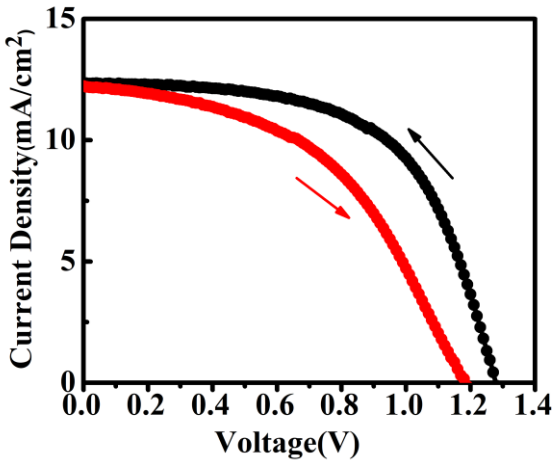

Figure S8 J-V curve of $CsPb_{0.8}Ge_{0.2}I_2Br$ perovskite film with reverse scan and forward scan direction.

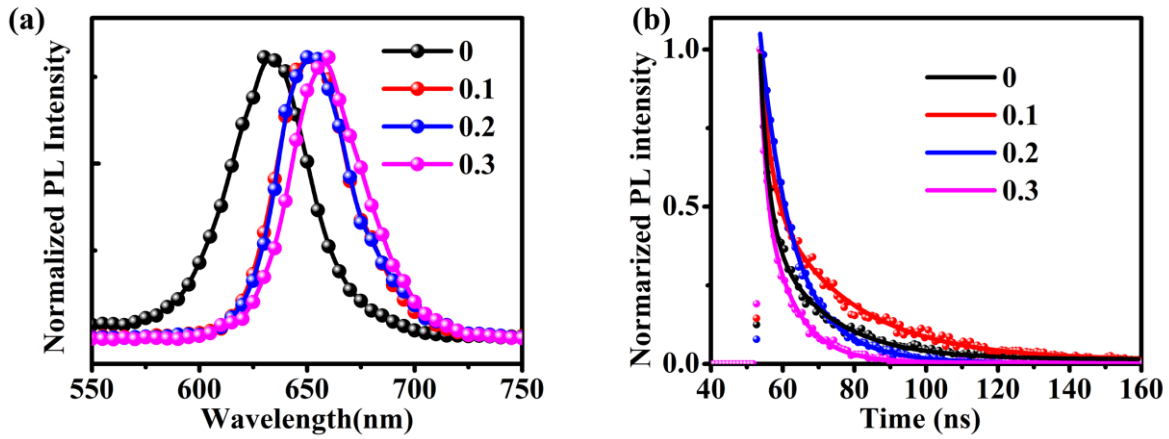

Figure S9 (a) Steady state PL spectra and (b) time-resolved PL spectra of annealed $CsPb_{1-x}Ge_xI_2Br$ perovskite film (x, 0, 0.1, 0.2, 0.3) Solid lines in (b) are the fitting curves using the double exponential decay model.

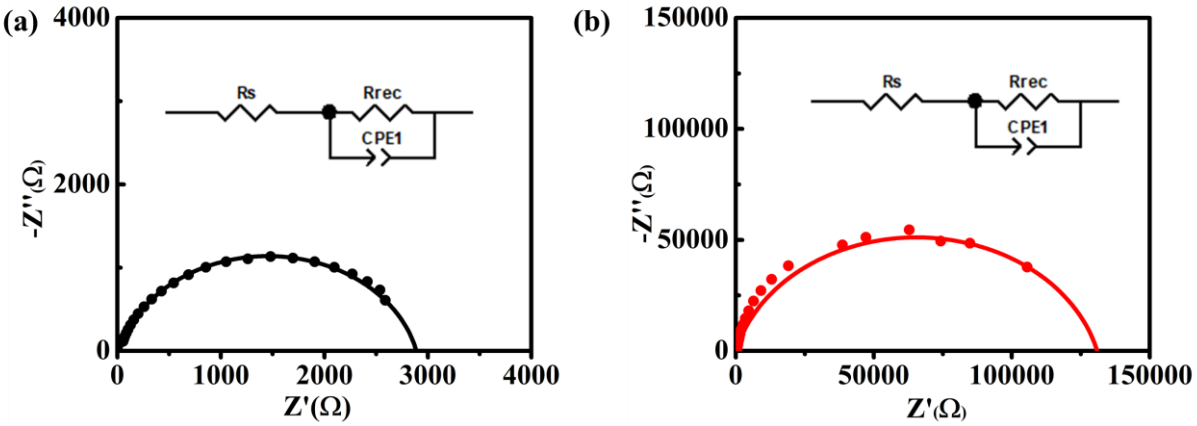

Figure S10 The Nyquist plots based planar perovskite devices measured in the dark under 0.7 V applied bias and the equivalent circuit diagram; the fitted curves and the experimental data are shown as solid lines corresponding points, respectively. (a) $CsPbI_2Br$, (b) $CsPb_{0.8}Ge_{0.2}I_2Br$.

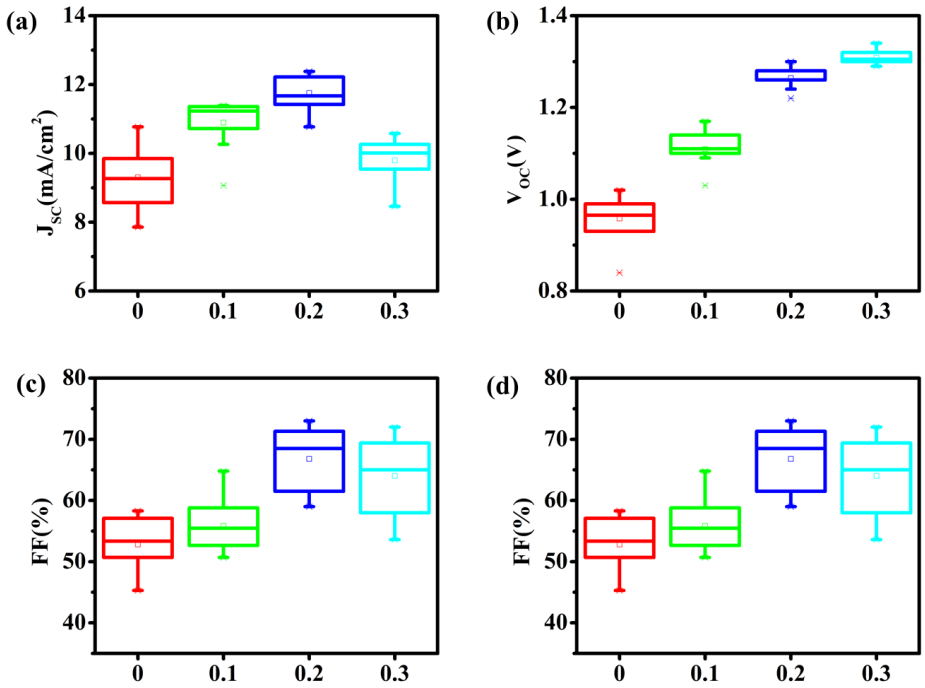

Figure S11 Photovoltaic statistics for the planar PSCs processed by $CsPb_{1-x}Ge_xI_2Br$ (x, 0, 0.1, 0.2, 0.3). (a) Short-circuit current, (b) Open circuit voltage, (c) FF, and (d) Efficiency. The boxes represent 80 data from the Voc-to-Jsc scan direction.

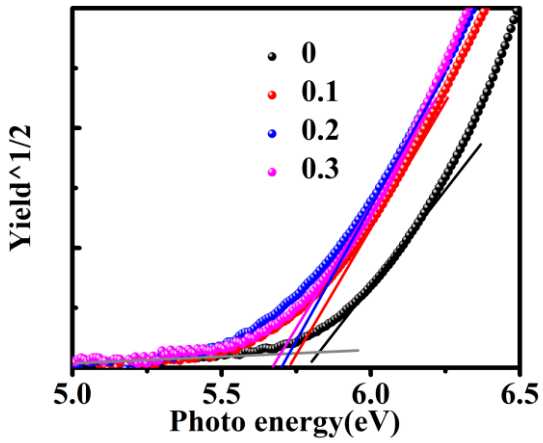

Figure S12 Valence band calculation for $CsPb_{1-x}Ge_xI_2Br$ perovskite film (x, 0, 0.1, 0.2, 0.3) measured by PYS.

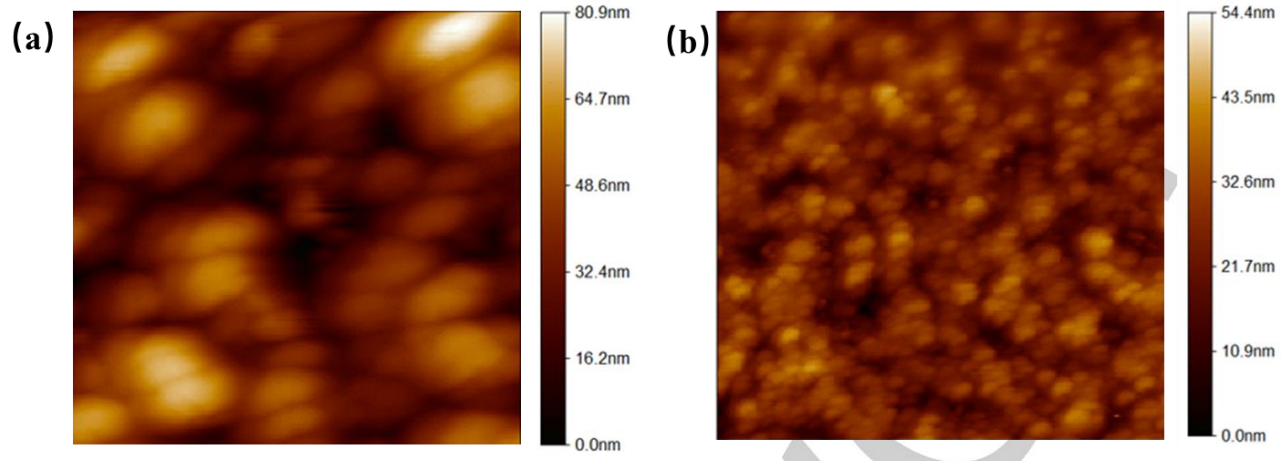

Figure S13 *AFM images of $CsPbI_2Br$ (a) and $CsPb_{0.8}Ge_{0.2}I_2Br$ perovskite film.*

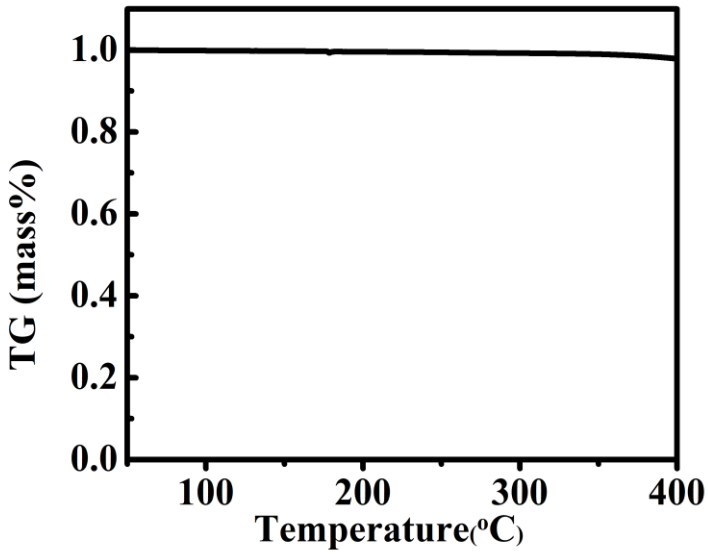

Figure S14 *Thermogravimetric analysis (TGA) curve of $CsPb_{0.8}Ge_{0.2}I_2Br$ perovskite.*

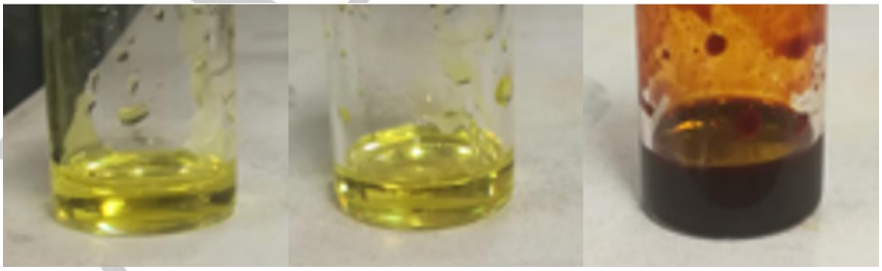

$CsPbI_2Br$ Fresh $CsPb_{1-x}Ge_xI_2Br$ Fresh $CsPbI_2Br+GeI_4$

Figure S14 Optical images of perovskite precusor solution.

x ratio	τ_1	A1	τ_2	A2
0	16.66	0.440	2.40	0.649
0.1	23.47	0.487	3.02	0.545
0.2	8.38	0.814	20.62	0.143
0.3	1.47	0.472	8.56	0.577

Table S1 Summary of the parameters fitted from the time-resolved PL spectra. The fitting function of the double-exponential equation was $y = y_0 + A_1 e^{-\frac{x}{\tau 1}} + A_2 e^{-\frac{x}{\tau 2}}$.

x ratio	FWHM	Crystallite size(nm)
0	0.122	69.7
0.1	0.241	35.3
0.2	0.261	32.6
0.3	0.357	23.8

Table S2 Crystallite size calculated using Scherer's formula using peak (110)